

FABRICATION OF MICRO-OPTICAL DEVICES

W. W. Anderson, J. Marley, and G. Gal
Lockheed Palo Alto Research Laboratory
3251 Hanover Street, Palo Alto, California 94304
and
D. Purdy
Philips Infrared Defense Components
Philips Components Limited
Southampton, Hampshire, SO9 7QG

ABSTRACT

We have fabricated a variety of micro-optic components including Fresnel and non-Fresnel lenses, off-axis and dispersive lenses with binary stepped contours and analog contours. Process details for all lens designs fabricated are given including multistep photolithography for binary fabrication and grayscale mask photolithography for analog fabrication. Reactive ion etching and ion beam milling are described for the binary fabrication process, while ion beam milling was used for the analog fabrication process. Examples of micro-optic components fabricated in both Si and CdTe substrates are given.

1.0 INTRODUCTION

We differentiate between two fabrication options for micro-optical components as binary and analog. Within each of these fabrication options, the components may be designed as Fresnel or non-Fresnel. These distinctions are illustrated in Figure 1. The discrete jumps in the Fresnel elements correspond to changes of 2π in phase. The thickness of Fresnel elements is $\lambda/(n-1)$, independent of element type, where n is the refractive index of the substrate material and λ is the design wavelength. The limited thickness of Fresnel elements relaxes the requirement of deep etching, but the Fresnel elements suffer from chromatic aberration.

The binary fabrication process derives its name from the sequence of process steps indicated in Figure 2 wherein a set of m photomasking and etching steps results in 2^m distinct levels. The photolithographic masks are either transparent or opaque. The analog fabrication process derives its name from the continuous curvature of the fabricated component which, in turn, derives its shape from the (almost) continuous grayscale optical density of a single photomask and the exposure/development process of positive photoresist.

The binary fabrication technology was originally described by d'Auaria et al.¹ Limitations of this technology include limitations on photolithographically definable feature size, accuracy of multiple masking step alignments, anisotropy of etching processes and maximum etching depths available. Several of these issues have been addressed in the past few years.²

An early version of analog fabrication of microlenses was described by Wada.³ Baking a small circular positive photoresist layer above the glass transition temperature was found to produce a spherical contour of the photoresist dot by the action of surface tension. The spherical contour was reproduced in the substrate by ion milling. This technique was limited to special shapes. In a positive photoresist system, the exposed areas become more soluble than the unexposed regions. By a grayscale exposure, the percentage of photoresist remaining after development is a function of exposure. Thus, ion milling of a substrate after exposure through a grayscale mask will replicate the photoresist profile in the substrate. Limitations of this technology include limitations on grayscale mask characteristics, differential etching characteristics of photoresist and substrate, and maximum etching depths available.

Both fabrication technologies require photolithography followed by anisotropic etching via reactive ion etching (RIE) or ion beam milling. The chemistry of RIE is quite substrate specific and so tends to be limited to the binary fabrication process wherein we wish to etch the substrate only and leave the masking layer intact. Ion milling, on the other hand, is a purely physical phenomenon in which the incoming ions are energetic enough to sputter material from the surface of the wafer. Thus the masking layer will be etched at a rate proportional to the substrate etching rate. Etching characteristics of both processes tend to be machine specific but once a machine is properly calibrated, the results are quite reproducible both with respect to depth versus time and anisotropy of etch.

A number of optical functions can be realized by properly designed and fabricated micro-optical components, as described in our companion papers.⁴⁻⁶ In this paper, we will describe our experience with the fabrication of a variety of micro-optics lenses by both analog and binary fabrication technologies.

2.0 BINARY FABRICATION

In this section, we describe the fabrication of simple microlens arrays for operation at a wavelength of 10.6 μm in both Si and CdTe substrate materials. In addition we will describe preliminary results on the fabrication of wideband and dispersive microlenses in CdTe. Two anisotropic etching technologies were utilized, RIE and ion beam milling. In addition, two separate masking sequences were used, fine-to-coarse and coarse-to-fine. The optical performance of the lenses is described in Reference 6.

1. d'Auaria, L., J. P. Huignard, A. M. Roy, and E. Spitz "Photolithographic Fabrication of Thin Film Lenses," *Opt. Commun.*, Vol. 5, 1972, pp. 232-235.
2. Stern, M. B., and S. S. Medeiros, "Deep Three-Dimensional Microstructure Fabrication for Infrared Binary Optics," *J. Vac. Sci. Technol.*, Vol. B 10, 1992, p. 2520.
3. Wada, O., "Ion-Beam Etching of InP and Its Application to the Fabrication of High Radiance InGaAsP/InP Light Emitting Diodes," *J. Electrochem. Soc.*, Vol. 131, 1984, p. 2372.
4. Gal, G., et al., "Micro-Optics Technology for Sensor System Applications," Conference on Binary Optics, Huntsville, AL, 1993.
5. Herman, B., and G. Gal, "Theory of Dispersive Microlenses," Conference on Binary Optics, Huntsville, AL, 1993.
6. Shough, D., B. Herman, and G. Gal, "Measurements of Microlens Performance," Conference on Binary Optics, Huntsville, AL, 1993.

The simple lens array mask consisted of a 16×16 lens array at the center of the mask, lens doublets widely spaced along orthogonal axes centered on the array, and single lenses sparsely populating the rest of the $12 \text{ mm} \times 12 \text{ mm}$ mask area. The singlets and doublets were for diagnostic purposes such as individual lens point-spread-function (PSF) measurement, nearest neighbor crosstalk determination, and large area uniformity evaluation. (A non-negligible consideration was the cost of a fully populated, e.g., 128×128 array, set of lens array masks.) In addition to the three-level mask set (which provided eight distinct phase steps modulo 2π), a light-blocking metallization mask was utilized to isolate the individual lens elements and arrays.

The master masks were 1X electron-beam generated using a $0.1\text{-}\mu\text{m}$ spot size. The substrate material was $4 \times 4 \times 0.6\text{-in.}$ quartz coated with antireflective chrome. Minimum feature size was $0.5 \mu\text{m}$. For this work, working plates were made from the masters. If feature sizes smaller than $0.5 \mu\text{m}$ were required, the quartz master plates would be used due to their low expansion coefficient and superior ultraviolet transmission characteristics. Each individual lens was $100 \mu\text{m} \times 100 \mu\text{m}$. Since the same mask set was used for Si and CdTe, the Si lens was designed to have a focal length of $525 \mu\text{m}$ and the CdTe lens to have a focal length of $420 \mu\text{m}$.

2.1 BINARY ETCHING

Anisotropic etching to depths of $\lambda/8(n - 1)$ to $\lambda/2(n - 1)$ is required. Uniformity of etching on the order of $\lambda/20$ is required over the entire lens array area. A step-wise approximation to a smooth profile may be fabricated by a multiple-step, binary-etching process as shown in Figure 2 for a positive photoresist. The anisotropic etching depths progress from $\lambda/8(n - 1)$ to $\lambda/2(n - 1)$ for the fine-to-coarse sequence shown in Figure 2. The same final profile could, in principle, be obtained by reversing the sequence to a coarse-to-fine order. In either sequence, multiple step lithographic processing will result in photoresist surface texturing the order of $\lambda/2(n - 1)$, which may degrade the photolithographic resolution attainable.

The etching must produce vertical side walls well registered with mask features (i.e., no undercutting or shadowing) or some lens area is lost. The etching must also produce smooth surfaces at the bottom of the etched area. Finally, the etch rate (or equivalently, etch depths) must be reproducible for a production process. The two technologies that satisfy these requirements are RIE and ion beam milling.

In RIE, ions produced in a plasma discharge react with a substrate material to form a volatile compound which is then removed from the system. The RIE process is highly anisotropic so that vertical side walls are obtained at the phase steps.

In ion beam milling, a collimated, uniform beam of inert ions, extracted from a plasma discharge, bombards the surface of a substrate. The momentum transferred by these ions breaks the bonds of the substrate surface atoms. Material not protected by a mask is selectively etched away. Etch features down to $0.2 \mu\text{m}$ and with aspect ratios of 5:1 can be achieved.

The chemistry of RIE for Si is well established so we used this technology for fabrication of Si components. The chemistry of CdTe is both more complex (a binary compound) and more primitive (limited level of developmental effort vis à vis Si) than that of Si, so the physical process of ion beam milling was used for the fabrication of CdTe components.

2.2 Si MICROLENS FABRICATION

Si substrate material specifications were: double-side optical-grade surfaces, $\langle 100 \rangle$ orientation (for RIE etching properties), 500 to $550\text{-}\mu\text{m}$ thickness (to place lens focal point near

opposite surface when illuminated from lens side), and resistivity $> 10 \Omega\text{-cm}$ (to minimize free carrier absorption at $10.6 \mu\text{m}$). The substrates were cleaned by soaking in a $\text{H}_2\text{SO}_4/\text{H}_2\text{O}_2$ bath at 120°C to remove organic residues. They were then immersed in a rinse tank of DI water until the water resistivity recovered to $> 10 \text{ M}\Omega$.

The Si micro-lenses were fabricated in a fine-to-coarse feature sequence as shown in Figure 2. A $2\text{-}\mu\text{m}$ -thick photoresist layer was an adequate etch mask for the first etch step of 550 nm . However, transfer masks of 250 and 500 nm CVD-deposited oxide were required for the second and third etching steps.

RIE was performed in a Plasma Therm 700 wafer/batch system using a Cl-based chemistry of $\text{SiCl}_4:\text{BCl}_3:\text{Cl}_2$ introduced into the etch chamber at $35:5:5\text{-sccm}$ flow rates. With a chamber base pressure of 20 mTorr , the Si etch rate was $\approx 46 \text{ nm/min}$. The Si to oxide selectivity etch rate was $10:1$ which determined the choice of the transfer mask oxide thicknesses mentioned above. The etch time for the fine feature mask did not polymerize the photoresist so it was easily stripped after etching. However, it was necessary to remove the photoresist from the oxide transfer masks prior to etching since the required longer etch times polymerized the photoresist making it difficult to remove.

In Figure 3 we show a low magnification scanning electron microscope (SEM) micrograph of the 16×16 array of Si microlenses to provide a qualitative indication of the uniformity achieved over the array. Note that individual lenses are of Fresnel type and are $100\text{-}\mu\text{m} \times 100\text{-}\mu\text{m}$ squares. The principal defects are isolated photoresist fragments. In Figure 4 we show a higher magnification SEM micrograph of the array at a 65° angle to reveal the depth profile. Of particular note are the 2π phase steps near the lens corners and the various characteristics of the edges associated with multiple masking and etching steps as indicated in Figure 2.

The 2π phase step is shown in the higher magnification SEM of Figure 5. Note the stratigraphic marks of the $\lambda/8$, $\lambda/4$, and $\lambda/2$ etching steps and their order in the 2π phase step wall. From Figure 2e we see that this wall was formed by first, the shallow $\lambda/8$ etch step, then the $\lambda/4$ etch step and finally the $\lambda/2$ etch step and, from Figure 2d, that there were two alignment steps after the initial shallow etch step. The other double alignment edge indicated in Figure 2d can result in rather distinct features associated with slight mask misalignment problems as shown in Figure 6a. If the subsequent masking steps for an edge are offset as indicated in Figure 6b, then trenching of the double alignment edge between levels 3 and 4 of Figure 2e and of the single alignment edge between levels 1 and 2 of Figure 2e are as predicted in Figure 6c and observed in Figure 6a.

2.3 CdTe MICROLENS FABRICATION

New low-temperature lithographic and ion milling process schedules were developed in order to be compatible with future dual-sided, integrated HgCdTe focal plane array processing. Samples of CdTe $1.5 \times 1.5 \text{ cm}$ were polished to an optical finish on both sides with $0.1\text{-}\mu\text{m}$ alumina abrasive to a flatness of less than three fringes. The samples were lapped to a thickness of $425 \mu\text{m}$. They were mounted on 5-cm polished sapphire substrates with paraffin and Turcowax-5580. This technique is intended to provide sample support throughout the entire fabrication procedure without remounting after each resist process. Ion milling of CdTe was accomplished using 500 V argon ions at a current density of 0.31 ma/cm^2 in a Technics Model 20 ion mill equipped with a cooled sample stage. Up to three samples could be pressure mounted against the water-cooled sample substrate holder which was positioned at an angle of 25° to the ion beam and rotated at 4 rpm . The sample temperature was monitored during milling using temperature-sensitive decals and maintained at a temperature below 80°C . These parameters resulted in a milling rate of 55 nm/min for CdTe.

Developed positive photoresist was used as the ion milling mask. Etch selectivity toward photoresist improves with increasing resist baking temperature. Since we limited our maximum process temperature to 80°C, the resist milling occurs at about 15 nm/min or an etch selectivity of about 3.7:1, CdTe to resist. In our standard process, the photoresist is baked at 120°C which results in an ion milling rate of about 10 nm/min or a selectivity ratio of about 5.5:1. A higher selectivity allows the use of a thinner resist schedule which, in turn, permits a more accurate pattern transfer. However, the lower selectivity does not seem to have had an adverse effect on our pattern replication. The lower process temperature results in easier resist stripping and less chance of resist distortion. Separate calibration runs were performed before each lens milling run. Milling depths were generally within $\pm 5\%$ of the target value, i.e., within $\lambda/20$.

In Figure 7 we show SEM photomicrographs of a CdTe broadband microlens array fabricated with the same set of masks used for the Si microlens array shown in Figures 3 through 6. (Figure 7 is directly comparable with Figure 4 for the Si array.) Gross quality of this array is comparable to that of the Si array. Higher magnification SEM micrographs reveal distinct differences in the wall features between RIE fabrication of Si and ion beam milling of CdTe. Trenching and redeposition during ion milling are well known⁷ and both are evident in the higher resolution SEM micrographs of the fracture cross section in Figure 8. Overall fabrication defects of $< 1 \mu\text{m}$ ($\lambda/10$) did not affect optical performance significantly. This lens produced near theoretical diffraction limited performance as described in Reference 6.

A set of nine microlens designs, including various combinations of pixel shapes and dispersive lenses of various orders and grating orientations, was developed and fabricated as a research test wafer to demonstrate the power of binary-fabricated micro-optics. Some of the lenses and arrays as fabricated by ion milling of CdTe are shown in Figures 9 and 10. The photomasks were divided into nine zones, one for each lens type. Each zone was partially populated with single lenses, doublets, 2×2 arrays, 4×4 arrays, and some special diagnostic arrays dependent on the particular lens design in each zone.

The dispersive lens mask set is a $1 \times$ E-beam generated master mask set, consisting of three layers for lens generation and a fourth layer for reflective metallization of areas outside the lenses. The patterns were written with a $0.1\text{-}\mu\text{m}$ E-beam spot size which resulted in a minimum resolvable feature size of 0.4 to $0.5 \mu\text{m}$. Submicron resolution was required on mask layer 3 since several lens types contained features as small as $0.8 \mu\text{m}$.

The small feature size required that we use the E-beam generated master masks for our contact photolithography process. The mask vendor was unable to print low defect chrome copies of the finest geometries contained on mask layer 3 because of too-small feature sizes. Results to date suggest that mask damage occurring from contact between mask and substrate is not currently a significant factor. Successful submicron feature resolution may be improved with better and more reproducible mask-to-substrate contact. This can usually be achieved by initially mounting the sample as flat as possible on the sapphire substrate carrier. An added advantage could be obtained by printing images with conformable masks. Near-perfect contact is easier to achieve if either the mask or the substrate is able to conform to the opposite member. Since the sapphire substrate is purposely chosen for its stiffness to minimize CdTe fracture, the mask must be the flexible element.

All the dispersive microlens fabrication has used AZ 5214-E positive resist since the AZ 5200 series product has submicron resolution capability and offers near-vertical profiles to give

7. Glöersen, P. G., "Ion-Beam Etching," *J. Vac. Sci. Technol.*, Vol. 12, 1975, p. 12.

accurate pattern transfer in ion beam etching applications. It also has high thermal stability to maintain resist profile quality in severe process environments. The smallest geometries are printed first on a completely planar surface so depth of field is not an issue. Also, no alignment is required on the first mask. Resist thickness is 1 to 1.5 μm . Layer 2 is also aligned under rather favorable conditions. The first milling step resulted in 0.75- μm -deep features in the CdTe surface and is the next most favorable surface for applying a thin, uniform resist layer for patterning the second layer using 1.5 μm of photoresist. After milling the second pattern the total surface topography is about 2.25 μm at the deepest feature which makes uniform resist coating and exposure of the third layer much more difficult. Line width narrowing due to over exposure of the top of narrow features as well as underexposure of the resist-covered trenches may result in broadening of the deepest features. Linewidth variations may also occur due to any layer-to-layer misalignment.

Successful printing of mask layer 3 on small samples of CdTe was anticipated to offer a very challenging process sequence, especially since the mask vendor was unable to fabricate chrome mask copies on ultraflat quartz plates under ideal conditions. However, the smallest features, namely 0.8- μm lines and spaces were successfully printed and developed on both CdTe and Si. The most difficult process steps have involved obtaining accurate mask registration over all nine zones simultaneously. Excessive resist reworking has often been required on some of the CdTe samples. This may be due in part to lack of flatness either on the sample surfaces or due to the mounting process on the sapphire wafers. We have found that repeated remasking can cause extensive sample damage by fracturing the finest features at the edges of lens arrays.

3.0 ANALOG FABRICATION

The analog fabrication of arbitrary topographies relies on the process characteristics of positive photoresists and the anisotropic etching characteristics of the ion milling process.

Positive resists contain a photosensitive dissolution inhibitor, an alkaline-soluble base polymer, and a solvent. The dissolution inhibitor prevents the base polymer from dissolving in the alkaline developer. After exposure to light, the dissolution inhibitor concentration is reduced in selected areas, leading to an increased solubility. The relevant characterization of the resist is a "characteristic curve," as shown in Figure 11, giving the percentage of resist remaining after development as a function of exposure. By exposing the photoresist through a grayscale mask⁸ such that the maximum exposure is less than the threshold exposure, E_0 , the quantity of photoresist remaining after development will be a one-to-one analog of the optical density of the mask. Obviously, the characteristic curve must be used to determine the optical density of the mask for a desired residual photoresist thickness.

Ion milling and rf-sputter etching have the capability of quite faithfully reproducing in relief in a substrate a pattern formed in photoresist on the substrate surface. Ion milling machines have been developed which allow control of incident ion beam angle, ion beam energy, and current density (or flux density if the beam has been neutralized). In Figure 12, if the etch rate of the resist is R_1 and the etch rate of the substrate is R_2 , then the total thickness of material removed is

$$\Delta(x) + \mu(x) = \Delta(x) + (t - \Delta(x)/R_1)R_2$$

8. Gal, G., "Method and Apparatus for Fabricating Microlens," under patent application, 1992.

as long as the etch time is sufficiently long to remove all of the photoresist, i.e., $t > \Delta(x)_{\max}/R_1$. The final substrate profile is then given by

$$h(x) = \Delta(x)/k + H - R_2t$$

where k is the relative etch rate of resist and substrate, $k = R_1/R_2$. Since photoresist typically mills at a rate of 20 nm/min and semiconductors at a rate of 40 nm/min, the relative milling rate, $k \approx 0.5 < 1$, and the milled topography will be an amplified version of the residual photoresist topography as indicated in Figure 12.

The fabrication of nonspherical surfaces such as a refractive/dispersive optic by standard techniques, such as the reflow of photoresist, have limited scope for further development. Consequently, it was necessary to develop a more flexible process. The adapted technique depends upon the exposure of a positive resist through a specially designed grayscale mask which was used to, in effect, photosculpt the surface relief pattern. Such a technique enables aspheric lens to be fabricated in a high-density matrix and is ideally suited to nonsymmetrical surfaces, such as the dispersive micro-optic. Modern electron beam mask writing systems can now achieve detail fine enough to enable half-tone-type images to be generated at a pixel size of 1- μm or less. The number of grayscales available from our mask design was 256. Current Philips designs contain nearly 1000 grayscale levels. This enables three-dimensional surfaces to be created with submicron accuracy and facilitates the production of the combined refractive/dispersive surface. This process eliminates the mask registration problem associated with binary fabrication and the too-small feature sizes required on multiple mask sets for an optic operating at short wavelengths (e.g., in the visible).

The first mask manufactured using this principle was a linear scale of stepped values used to calibrate the sensitivity of the resist and the resultant depth of exposure achieved for each gray level in the mask. Using this calibration for exposure depth versus gray value, a mask was produced where the contours of the refractive/dispersive optical design were encoded into gray values at each spatial coordinate of pixel steps in the x and y directions. The resultant mask was used on a 10:1 stepper to expose a resist layer of suitable thickness. Development of the resist revealed an array of lens images which were ready to be transferred into the supporting substrate. The thickness of this substrate matched the focal length of the optical design and, after transfer of the resist image, the optic needed no further work to complete it.

The transfer of the resist image uses ion beam milling where all the parameters were controlled in such a way that the resist is made to erode at the same rate as the underlying substrate in an anisotropic fashion, i.e., $k = 1$ from the discussion above. Two SEM views of the finished lens are shown in Figure 13. Note the smooth contour of the analog surface vis à vis the highly textured surfaces of the binary-fabricated lenses shown in Figures 9 and 10.

The optical components were fabricated and tested by Philips for their ability to disperse infrared radiation from a 500 K blackbody. Detection of the position of the dispersed radiation was made by comparing the spectral response curves taken from each element in a linear array of small detectors spaced at 20- μm pitch. The optical elements were mounted in contact with this detector array. The pitch between the optical elements was 85 μm and, therefore, the resultant vernier effect enabled the dispersion effect to be evaluated in some detail. The cutoff wavelength of the array was 12 μm at 77 K and a shift of peak sensitivity from 8 to 12 μm was observed over a linear distance of about 50 μm on the focal plane.

4.0 SUMMARY

We have described the fabrication of a number of micro-optic components, both Fresnel and non-Fresnel, broadband and dispersive, by binary and analog techniques. The advantages and disadvantages of the various fabrication technologies are summarized in Table 1 where + indicates a preferred advantage, ++ indicates a significant advantage, - indicates a difficulty, and -- indicates a significant difficulty.

	ANALOG	BINARY
NON-FRESNEL		
FRESNEL		

FIGURE 1. MICRO-OPTIC COMPONENT DESIGN AND FABRICATION OPTIONS.

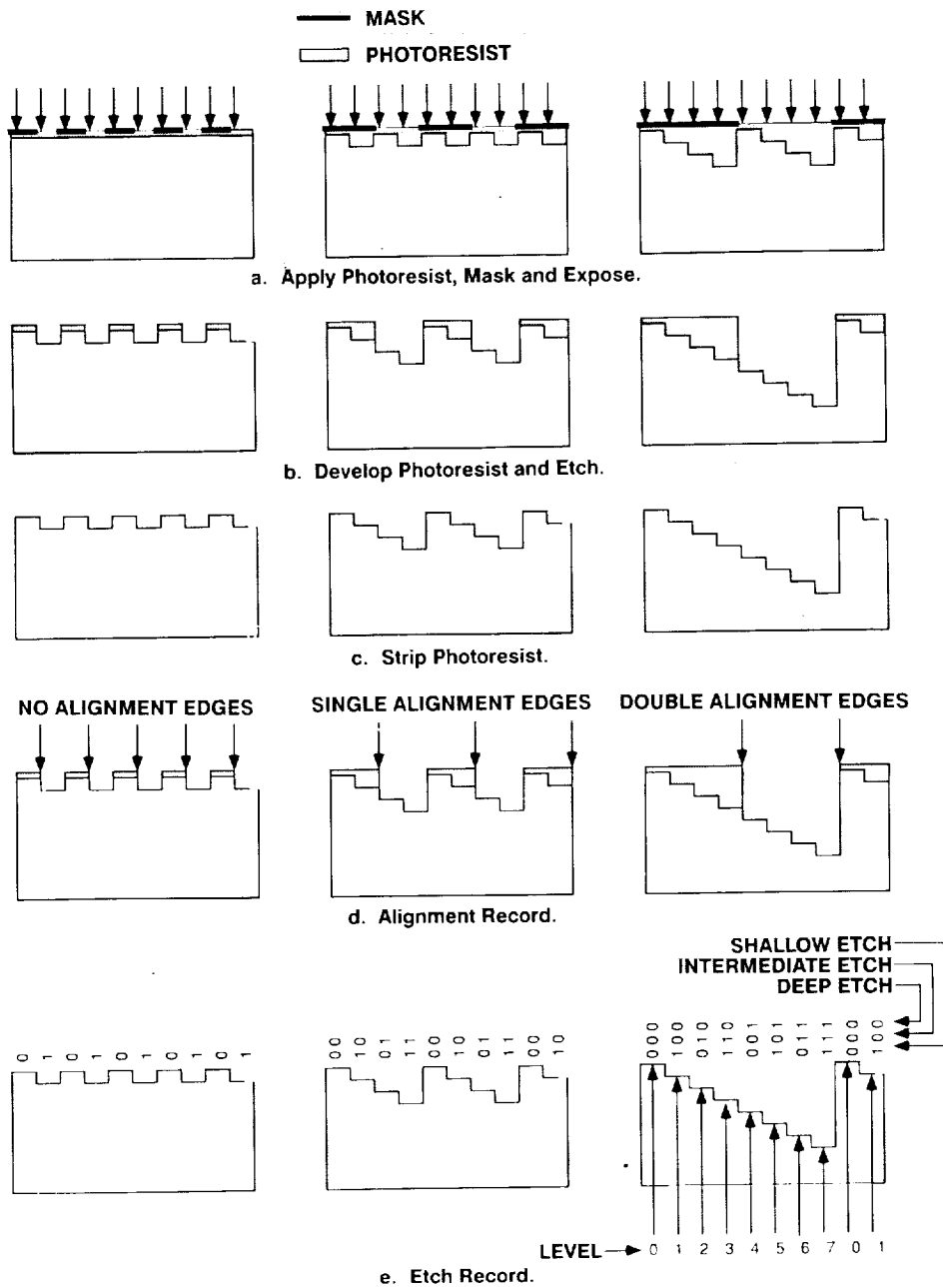


FIGURE 2. BINARY MICRO-OPTIC FABRICATION SEQUENCE.

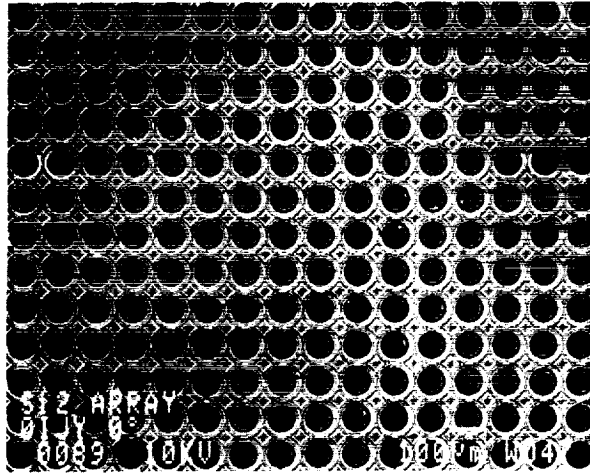


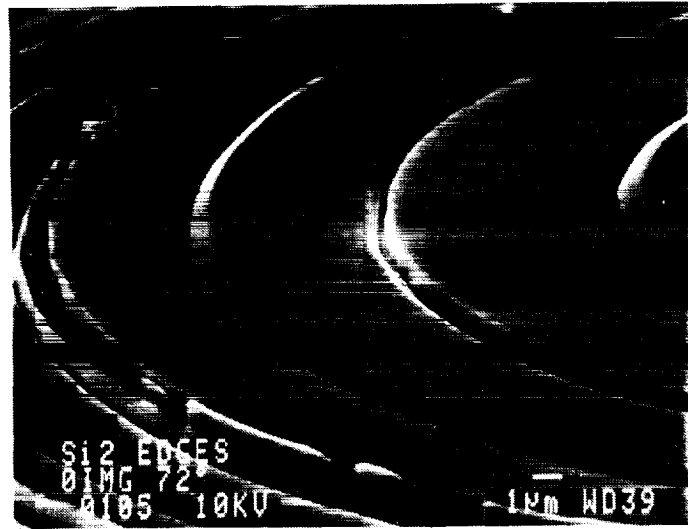
FIGURE 3. SEM MICROGRAPH OF 16×16 ARRAY OF Si MICROLENSES FABRICATED BY REACTIVE ION ETCHING.



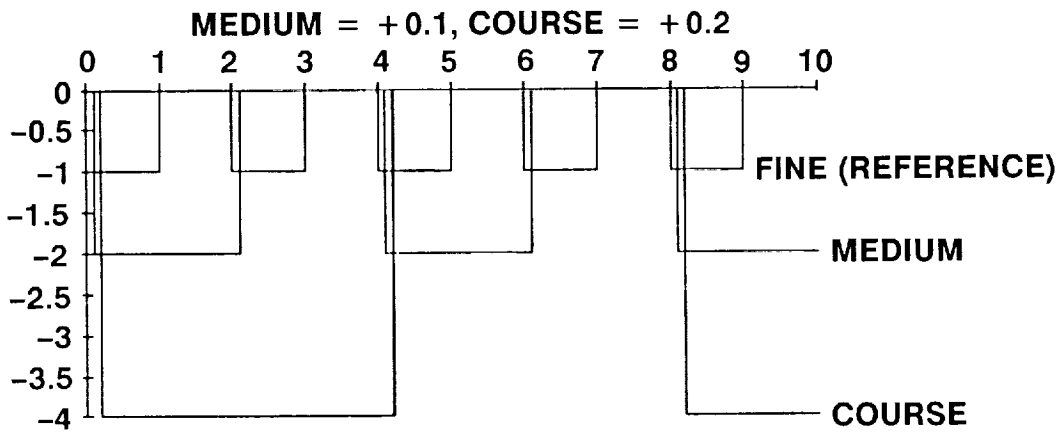
FIGURE 4. SEM MICROGRAPH OF Si MICROLENS ARRAY AT 65° ANGLE. Note 2π phase step at individual lens corners.



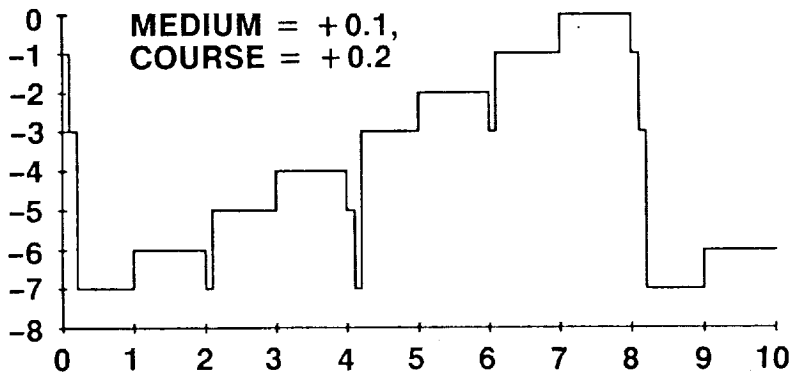
FIGURE 5. SEM MICROGRAPH OF 2π PHASE STEP. Note stratigraphic marks of $\lambda/8$, $\lambda/4$ and $\lambda/2$ etching steps in 2π wall.



a. SEM Micrograph of Multiple Step Alignments and Etching.



b. Relative Mask Alignments.



c. Resultant Etching Profile.

FIGURE 6. EFFECTS OF MISALIGNMENT IN MULTIPLE STEP BINARY MASKING OPERATIONS.

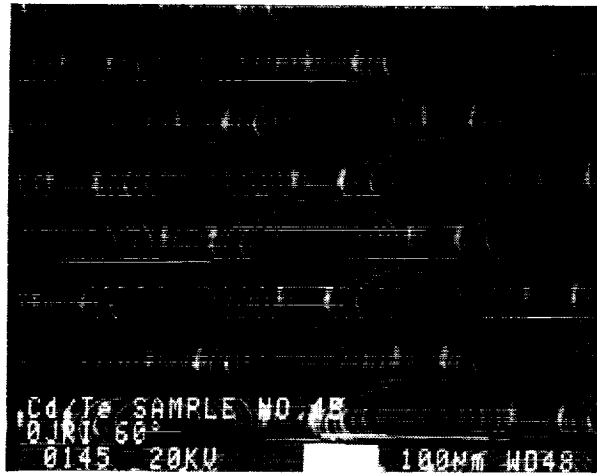
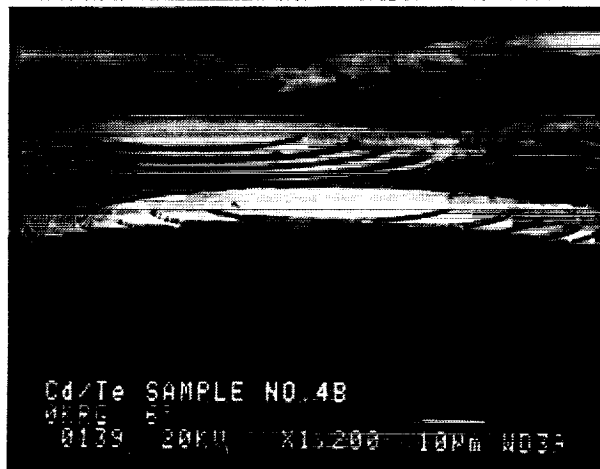


FIGURE 7. SEM MICROGRAPH OF CdTe MICROLENS ARRAY AT 65° ANGLE. Note 2π phase step at individual lens corners.



a. SEM Micrograph of CdTe Microlens Fracture Cross Section.

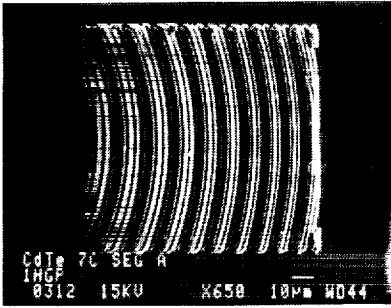


b. Detail of Ion Beam Etched Wall.

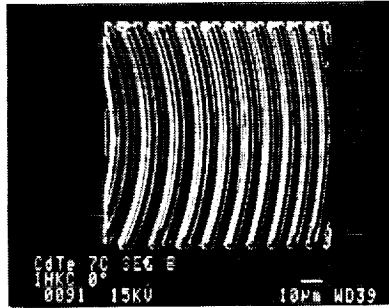
FIGURE 8. CHARACTERISTICS OF BINARY PHASE STEPS IN WALLS OF CdTe MICROLENS FABRICATED BY ION BEAM MILLING.

3 MASKS 8 LEVELS

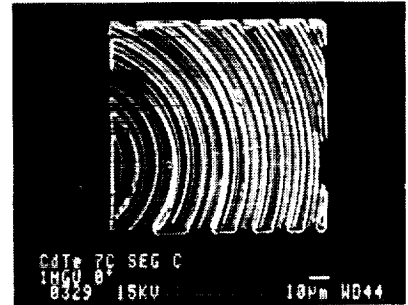
$m = 1$



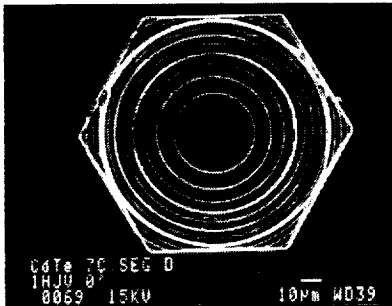
$m = 2$



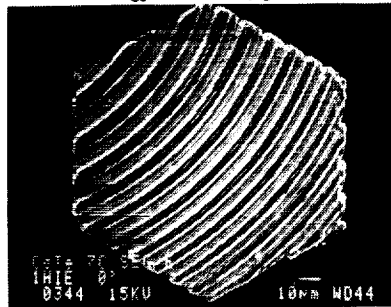
$m = 1$
 $\alpha = +11.5^\circ$



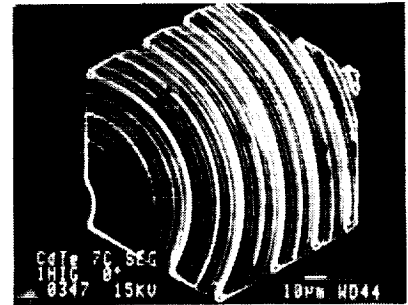
WIDEBAND



$m = 2$
 $\alpha = -19^\circ$



$m = 1$
 $\alpha = -19^\circ$



SKEWED

$\theta = 11.5^\circ$ $\alpha = 11^\circ$ $m = 1$

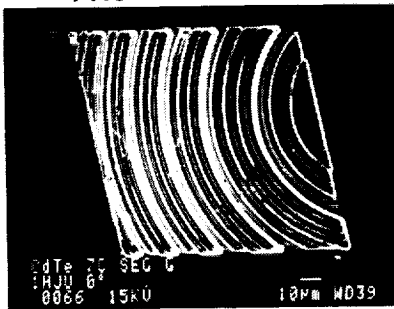
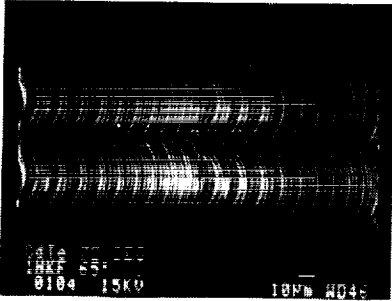


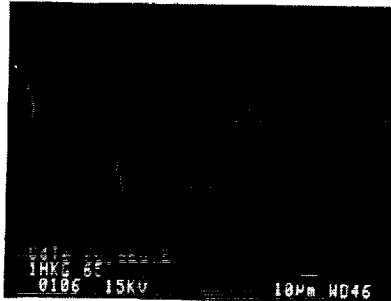
FIGURE 9. EXAMPLES OF BINARY FABRICATED WIDEBAND AND DISPERSIVE MICROLENSSES FORMED IN CdTe.

3 MASKS 8 LEVELS

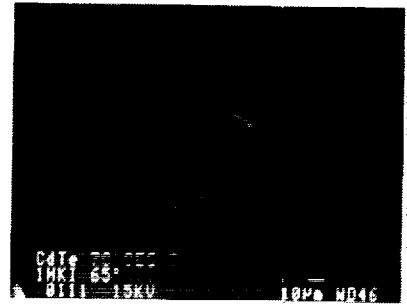
$m = 1$



$m = 2$



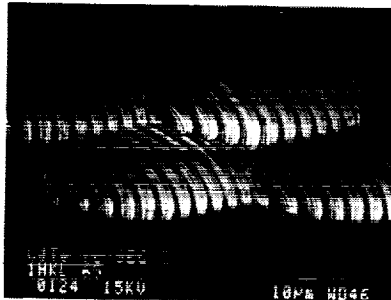
$m = 1$
 $\alpha = +11.5^\circ$



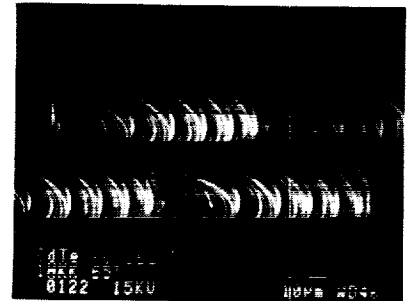
WIDEBAND



$m = 2$
 $\alpha = -19^\circ$



$m = 1$
 $\alpha = -19^\circ$



SKEWED

$\theta = 11.5^\circ$ $\alpha = 11^\circ$ $m = 1$



FIGURE 10. ARRAYED WIDEBAND AND DISPERSIVE MICROLENSES IN CdTe.

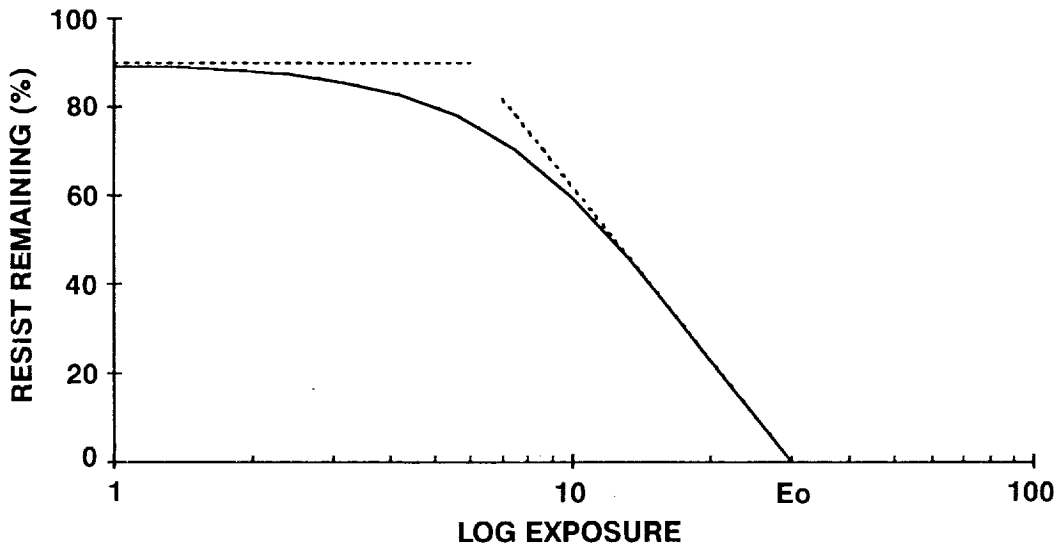


FIGURE 11. CHARACTERISTIC CURVE FOR A POSITIVE RESIST.

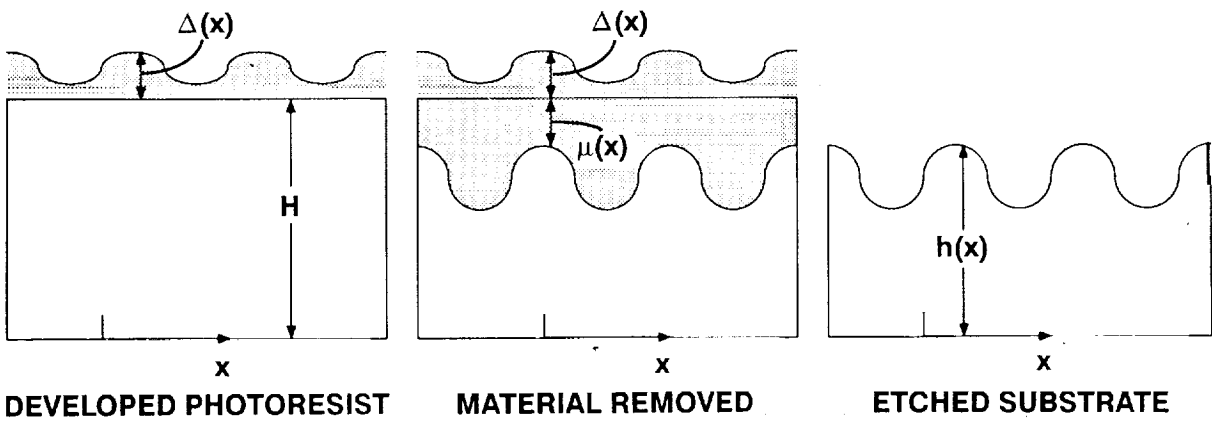


FIGURE 12. PHOTORESIST TOPOGRAPHICAL PATTERN TRANSFER BY ION MILLING.

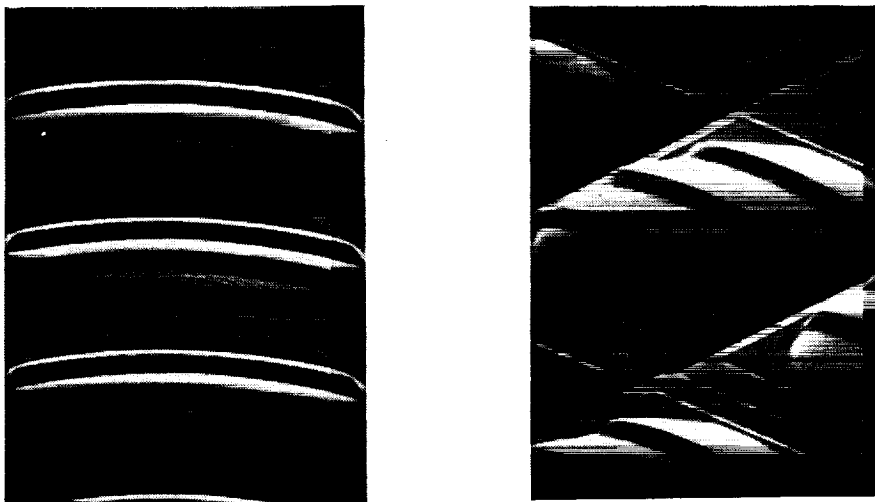


FIGURE 13. TWO SEM VIEWS OF ANALOG FABRICATED DISPERSIVE MICROLENS.

1. The first part of the document discusses the importance of maintaining accurate records of all transactions. It emphasizes that proper record-keeping is essential for the integrity of the financial system and for the ability to detect and prevent fraud. The text notes that without reliable records, it would be difficult to track the flow of funds and identify any irregularities.

2. The second part of the document focuses on the role of internal controls in ensuring the accuracy of financial reporting. It describes how internal controls are designed to prevent errors and misstatements, and to ensure that all transactions are properly authorized and recorded. The text highlights the importance of a strong internal control system in maintaining the trust of investors and other stakeholders.

3. The third part of the document discusses the impact of external audits on the financial statements. It explains that external audits provide an independent assessment of the company's financial position and the accuracy of its financial reporting. The text notes that a clean audit opinion is a key indicator of the company's financial health and reliability.

4. The fourth part of the document addresses the challenges of financial reporting in a complex and rapidly changing environment. It discusses the need for transparency and disclosure of all material information, and the importance of staying up-to-date on the latest accounting standards and regulations. The text also mentions the role of technology in improving the efficiency and accuracy of financial reporting.

5. The fifth part of the document discusses the importance of ethical behavior in the financial industry. It emphasizes that ethical conduct is essential for maintaining the trust and confidence of the public. The text notes that unethical behavior, such as fraud and insider trading, can have serious consequences for the financial system and the economy as a whole.

6. The sixth part of the document discusses the role of government in regulating the financial industry. It explains that government intervention is necessary to ensure the stability and integrity of the financial system. The text notes that government regulations, such as the Sarbanes-Oxley Act, are designed to protect investors and the public from the risks of financial fraud and mismanagement.

7. The seventh part of the document discusses the importance of financial literacy for the general public. It explains that financial literacy is essential for making informed decisions about money and investments. The text notes that financial literacy programs can help individuals understand the basics of finance and avoid common financial pitfalls.

8. The eighth part of the document discusses the future of the financial industry. It notes that the industry is facing significant challenges, such as the rise of fintech and the increasing demand for transparency and accountability. The text suggests that the industry must embrace change and innovation to remain relevant and successful in the future.